INTERNATIONAL JOURNAL OF CLIMATOLOGY
Int. J. Climatol. **37** (Suppl.1): 59–74 (2017)
Published online 25 January 2017 in Wiley Online Library
(wileyonlinelibrary.com) DOI: 10.1002/joc.4976

RMetS
Royal Meteorological Society

Potential effects of land cover change on temperature extremes over Eurasia: current *versus* historical experiments

Xing Li,[a,b] Haishan Chen,[a,b]* Hong Liao,[b,c] Wenjian Hua,[a,b] Shanlei Sun,[a,b] Hedi Ma,[a,b] Xiao Li,[a,b] Chujie Gao[a,b] and Siguang Zhu[d]

[a] *Collaborative Innovation Center on Forecast and Evaluation of Meteorological Disasters/Key Laboratory of Meteorological Disaster, Ministry of Education, Nanjing University of Information Science & Technology (NUIST), China*
[b] *International Joint Research Laboratory on Climate and Environment Change (ILCEC), Nanjing University of Information Science & Technology (NUIST), China*
[c] *School of Environmental Science and Engineering, Nanjing University of Information Science & Technology (NUIST), China*
[d] *College of Global Change and Earth System Science, Beijing Normal University, China*

ABSTRACT: Land use and land cover change (LUCC) is an important external forcing agent of climate change. The comparison of current (2000 A.D.) with historical (1850 A.D.) land cover maps suggests that most of the Eurasian continent has experienced robust and significant LUCC during the past century, especially evident transition from forests to croplands. Therefore, two experiments (control and sensitivity experiments with current and historical land cover maps, respectively) are conducted by using the Community Atmosphere Model Version 5.0 (CAM5.0) coupled with the Community Land Model Version 4.0 (CLM4.0) to investigate the potential effects of LUCC on temperature extremes over Eurasia. Results show significant increases (e.g., 0.2–0.7 °C) in extreme cold indices (e.g., TNn) over central and eastern China, India and mainland Southeast Asia in response to such robust LUCC. Broad and significant decreases (e.g., approximately −1 °C) in extreme warm indices (TXx) are mainly observed in Eastern Europe and western Siberia. Moreover, the effects of LUCC on high and low-percentile extreme indices of minimum temperature (T_{min}) are generally symmetrical, but those for maximum temperature (T_{max}) indices are asymmetrical, which are characterized by stronger influences on high-percentile indices rather than low ones. Further analyses suggest that LUCC-induced changes in temperature extremes are mostly influenced by shifts in the mean state of T_{min}/T_{max}. Furthermore, the responses and sensitivities of T_{min}/T_{max} to LUCC are remarkably distinct among regions. This result mainly occurs because of different LUCC-induced changes in surface energy components, which depend on the region-specific climatology of each energy component and the dominant plant functional types.

KEY WORDS land use and land cover change; temperature extremes; climate modelling; Eurasia

Received 11 May 2016; Revised 2 December 2016; Accepted 2 December 2016

1. Introduction

According to the Fifth Assessment Report of Intergovernmental Panel on Climate Change (IPCC AR5), human activities have caused a variety of irreversible changes in the Earth's climate system in the past, the present and probably the future (Myhre *et al.*, 2013). In the context of global warming, a great increase in extreme hot events has been observed in recent decades (Alexander *et al.*, 2006; Donat *et al.*, 2013a, 2013b), which are likely associated with human activities (Hegerl *et al.*, 2004; Christidis *et al.*, 2011; Seneviratne *et al.*, 2012; Sun *et al.*, 2014) and will continue if this warming trend is sustained (Tebaldi *et al.*, 2006; Orlowsky and Seneviratne, 2012; IPCC, 2012; Sillmann *et al.*, 2013b; IPCC, 2013; Seneviratne *et al.*, 2014). In addition to greenhouse gases (GHGs) and aerosols, land use and land cover change (LUCC) is another complicated and important forcing agent that is induced by human activities and has been proven to play a non-negligible role on the climate system (Claussen *et al.*, 2001; Foley *et al.*, 2005; Pielke, 2005; Pielke *et al.*, 2011; Pongratz *et al.*, 2010; Lawrence *et al.*, 2012; He *et al.*, 2014; Mahmood *et al.*, 2014, Hua *et al.*, 2015a, 2015b; Lawrence and Vandecar, 2015).

Unlike greenhouse gases, which induce irrefutable and remarkable warming effects on the global and regional climate, the signs and amplitudes of LUCC impacts on the mean temperature are greatly regionally dependent (Bounoua *et al.*, 2002; Feddema *et al.*, 2005; Bonan, 2008; Lawrence and Chase, 2010; de Noblet-Ducoudré *et al.*, 2012) and exhibit large uncertainties (Pitman *et al.*, 2009; Hua and Chen, 2013a; Hirsch *et al.*, 2015). However, LUCC-induced diurnal temperature range (DTR) changes are more consistent and robust than the mean temperature (Voldoire and Royer, 2004), e.g., a trend of the DTR (−0.105 °C per decade) being at least thrice as high as that of the mean temperature (+0.027 °C per decade) in the

* Correspondence to: H. Chen, International Joint Research Laboratory on Climate and Environment Change, Nanjing University of Information Science & Technology (NUIST), Ningliu Road 219, Nanjing 210044, China. E-mail: haishan@nuist.edu.cn

United States (Kalnay and Cai, 2003). Zhou *et al.* (2004) obtained similar conclusions regarding an LUCC-induced strongly decreasing trend in the DTR (−0.132 °C per decade) but a weakly increasing trend in the mean temperature (+0.050 °C per decade) during winter over Southeast China. Furthermore, consistent results in the aforementioned findings have been revealed by numerous modelling studies (Gao *et al.*, 2007; Lawrence and Chase, 2010; Hua and Chen, 2013b; Xu *et al.*, 2015).

DTR is an intuitional extreme temperature index, so these robust LUCC-induced DTR changes suggest more prominent effects of LUCC on extreme temperatures than on the mean temperature (Voldoire and Royer, 2004). Some studies that focused on this issue discussed the effects of LUCC on temperature and rainfall extremes. For example, Avila *et al.* (2012) stated that LUCC plays an equivalently important role in regional temperature extremes compared to doubling the carbon dioxide (CO_2) concentration, which has also been confirmed by Pitman *et al.* (2012) based on multi-model simulations. Christidis *et al.* (2013) used an optimal fingerprinting technique and found that LUCC signals can be detectable in observed global mean warm extremes, which is not the case for cold extremes. Hu *et al.* (2010) estimated the effect of land surface changes on extreme temperature over eastern China and concluded that land surface changes can explain approximately one third (nearly half) of the observed annual warm (cold) nights trend.

The land cover over Eurasia has experienced enormous changes over the past centuries because of human activities (e.g., deforestation, cultivation and urbanization) (Ramankutty and Foley, 1999; Goldewijk, 2001; Pielke *et al.*, 2011). Changes in large-scale land cover – an external forcing would influence the radiative forcing of climate system – could alter the likelihood of extreme temperature events (IPCC, 2013). Recently, more frequent extreme events have been detected over the Eurasian continent in addition to rapidly increasing temperatures (Donat *et al.*, 2013a, 2013b; IPCC, 2013). However, the causes of warming trends and the increasing variability of extreme events remain unclear. Some research has examined the potential influence of LUCC on extreme climates from a global scale/global mean perspective, and temperature extremes are generally agreed to be affected by global LUCC (e.g., Avila *et al.*, 2012; Pitman *et al.*, 2012; Christidis *et al.*, 2013), but these studies still lack further explanations. Nevertheless, the relevant mechanisms of changes in temperature extremes over regions with different spatial-temporal scales and intensities of LUCC are rarely paid enough attention. In addition, the recent IPCC Special Report (IPCC, 2012) noted that climate extremes could be linked to changes in their mean values, variances, and/or shapes of the probability distribution (SPD; Seneviratne *et al.*, 2012). Hence, the role that LUCC-induced changes in the mean states of the minimum (T_{min}) and maximum temperature (T_{max}) play in extremes variations will also be examined in this study. As such, the present study aims to (1) investigate the potential effects of LUCC on temperature extremes over Eurasia based on an atmospheric general circulation model that is coupled with a land surface model and (2) improve our understanding regarding possible mechanisms from the perspective of the role of changes in the mean T_{min} and T_{max} on extreme events. This study begins with a description of the model, experiments and methods in Section 2. Section 3 presents the main results of this study. Further investigations on the effects of LUCC-induced mean T_{min} and T_{max} changes on temperature extremes and the possible mechanisms are detailed in Section 4. Section 5 concludes our findings with discussions.

2. Model and methodology

2.1. Model and experiments

The models that are used in this study are the National Center for Atmospheric Research's Community Atmosphere Model Version 5.0 (NCAR CAM5.0) (Neale *et al.*, 2012) and Community Land Model Version 4.0 (CLM4.0) (Oleson *et al.*, 2010), which are the atmosphere and land components of NCAR's Community Earth System Model (CESM), respectively (Gent *et al.*, 2011). The CESM and the previous version of the Community Climate System Model (CCSM) have been widely used to study the climatic effects of LUCC (Lawrence *et al.*, 2011, 2012; Xu *et al.*, 2015). The NCAR's models (i.e., NCAR CCSM4 and CESM1) are also a part of the CMIP5 models and have been proven to reasonably simulate temperature and precipitation extremes in the present climate (Sillmann *et al.*, 2013a; Dong *et al.*, 2015). CAM5.0 is configured with a finite-volume dynamical core (details can be found in Chapter 3 of Neale *et al.*, 2012) at a horizontal resolution of $1.9° \times 2.5°$ and 26 layers of hybrid $\sigma - p$ (sigma-pressure) coordinates in the vertical direction. CLM4.0 is also configured with a horizontal resolution of $1.9° \times 2.5°$, five layers of snow and 15 layers of soil. CLM4.0 includes 17 plant functional types (PFTs), i.e., eight trees, three grasses, three shrubs, two crop types, and bare ground. In addition, the climatological monthly sea surface temperature (SST) and sea ice extent are prescribed in the model as ice–ocean boundary conditions, respectively.

Two simulations were conducted to examine the possible effects of LUCC on extreme temperatures: a control run (LU2000) with fixed current land cover (2000 A.D.) and a sensitivity experiment (LU1850) that was driven by historical land cover (1850 A.D.). Note that LUCC in these simulations is considered on a global scale. The historical land cover data that were used in this study were reconstructed by Hurtt *et al.* (2009, 2011) for the period 1500–2100, which can be downloaded from http://cmip-pcmdi.llnl.gov/cmip5/forcing.html#land-use_data. This dataset, which is based on a Global Land-Use model (Hurtt *et al.*, 2006), was generated with the HYDE database V3.1 (Goldewijk *et al.*, 2011) and updated estimates of historical national wood harvest, and shifting cultivation. Additionally, this historical land cover dataset was recommended by CMIP5 (Coupled

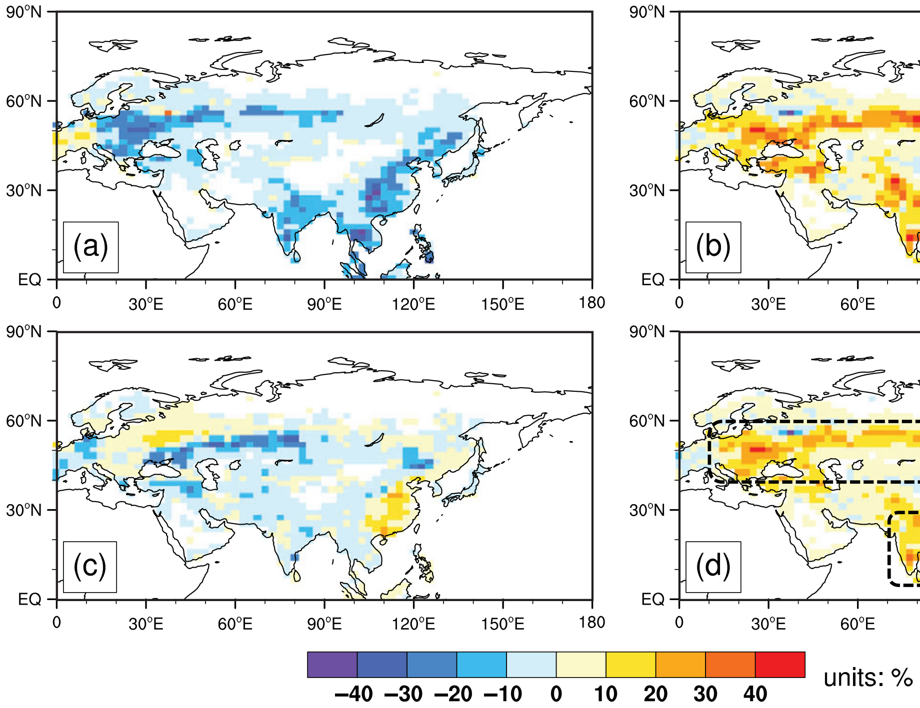

Figure 1. The fractional change in plant functional types (pfts) between historical and current land cover in two experiments (LU2000 − LU1850) over Eurasia: (a) forest, (b) crop, (c) grass, (d) (crops-forests)/2. Here, forest, crop and grass percentage are calculated as sum of all eight types of trees, two types of crops and three types of grass, respectively. Three regions of intensive LUCC (convert from forest-to-crop) are also shown in (d): India and mainland southeast Asia (approximately 70°–105°E, 5°–30°N; short for ISEA), central and east China (100°–120°E, 20°–40°N; short for CAEC) and east Europe and west Siberia (10°–100°E, 40°–60°N; short for EUWS).

Model Intercomparison Project Phase 5) and has been imported into the Community Climate System Model Version 4.0 (CCSM4.0) through developing new functionality in CLM4.0 (Lawrence *et al.*, 2012). Both LU2000 and LU1850 runs were forced by prescribed present day (1982–2001) climatological sea surface temperatures (SST) and sea ice extents of the 1° Hadley Center datasets (HadISST), and both integrate a 62-year period from 1951 to 2012. All the other forcing agents in both simulations were fixed at 2000 A.D. or the climatology level (e.g., CO_2 of approximately 367 ppm and total solar irradiance of approximately 1366.092 W m^{-2}). The results during the period of 1961–2012 were only used for the analyses (the first 10 years were considered a spin-up period and were not included).

Figure 1 shows the fractional differences in the three major PFTs (i.e., forests, crops and grasses) between the two experiments (LU2000 minus LU1850) over Eurasia. The percentages of forests, crops and grasses were calculated as the sum of all types of trees, crops and grasses, respectively. The historical LUCC mainly occurred in three major regions: India and mainland Southeast Asia (70°–105°E, 5°–30°N; ISEA hereafter), central and eastern China (100°–120°E, 20°–40°N; CAEC hereafter) and Eastern Europe and western Siberia (10°–100°E, 40°–60°N; EUWS hereafter). Additionally, the characteristics of the LUCC over these three regions were mainly featured by deforestation and cropland expansion (Figures 1(a) and (b)). However, the changes in grasses were much smaller than those in forests and cropland (Figure 1(c)). Thus, the forest-to-crop changes were approximately (Δcrop − Δforest)/2 [Δcrop (Δforest) denotes the fractional differences in crops (forests) between 2000 A.D. and 1850 A.D.]. As depicted in Figure 1(d), regions with strong LUCC experienced forest-to-crop changes of more than 20%. Thus, this study only focuses on regions with specific conversions of forests to crops (i.e., ISEA, CAEC and EUWS) in the following sections.

2.2. Climate extreme temperature indices

According to the recommendations by the CCI/CLIVAR/JCOMM Expert Team on Climate Change Detection and Indices (ETCCDI; Alexander *et al.*, 2006), 15 extreme temperature indices were selected to represent temperature extremes, including four absolute indices, four percentile-based indices, four threshold indices and three duration indices (detailed information in Table 1). Zhang *et al.* (2011) stated that the ETCCDI indices were useful and effective to assess climate extreme changes in both observations and modelling. Notably, we used the period of 1971–2000 from the LU2000 experiment as a reference period to obtain the thresholds of various temperature extremes. According to the given thresholds, all the extreme temperature indices from the LU1850 and LU2000 experiments could be extracted with daily T_{min} and T_{max}. Lastly, the multi-year annual mean difference in each extreme temperature index between LU2000 and LU1850 (LU2000 − LU1850) was estimated to quantify the effects of LUCC on temperature extremes.

Table 1. The definitions of the extreme temperature indices used in this study.*

Type	Index	Definition	Unit
Absolute indices	TNn	Monthly minimum value of daily T_{min}	°C
	TNx	Monthly maximum value of daily T_{min}	°C
	TXn	Monthly maximum value of daily T_{max}	°C
	TXx	Monthly maximum value of daily T_{max}	°C
Percentile-based indices	TN10P	Numbers of days when T_{min} < 10th percentile	days/year
	TN90P	Numbers of days when T_{min} > 90th percentile	days/year
	TX10P	Numbers of days when T_{max} < 10th percentile	days/year
	TX90P	Numbers of days when T_{max} < 90th percentile	days/year
Threshold indices	FD	Number of days when $T_{min} < 0$ °C	days/year
	TR	Number of days when $T_{min} > 20$ °C	days/year
	ID	Number of days when $T_{max} < 0$ °C	days/year
	SU	Number of days when $T_{max} > 25$ °C	days/year
Duration indices	CSDI	Annual count of days with at least six consecutive days when T_{min} < 10th percentile	days/year
	WSDI	Annual count of days with at least six consecutive days when T_{min} > 90th percentile	days/year
	GSL	Annual count between first span of at least six days with daily mean temperature $T > 5$°C and first span after July 1st of 6 days with $T < 5$°C.	days/year

*More details can be found on http://etccdi.pacificclimate.org/list_27_indices.shtml, T_{min}: minimum surface air temperature, T_{max}: maximum surface air temperature, T: mean surface air temperature.

A two-tailed Student's *t*-test was employed to measure the statistical significance level of these differences. It should be noted that in this study, we specified SPD (e.g., skewness) changes as all the changes in the probability density function excluding the mean state and variance changes, but non-mean-state changes as the changes in variance and SPD.

3. Results

3.1. Effects of LUCC on the mean maximum and minimum temperature

We begin with a brief comparison of the annual mean state of T_{min} and T_{max} between LU1850 and LU2000 over Eurasia, which is referred to as LU2000 − LU1850 (Figure 2), to better understand changes in temperature extremes that are induced by LUCC. Although we observed broad cooling over Eurasia that was mainly located to the north of 50°N, the magnitude of the LUCC-induced cooling effect was slight (approximately −0.4 to 0 °C) and not significant in terms of the mean responses of T_{min}. By contrast, most of the areas to the south of 50°N exhibited various increases in T_{min}. For instance, a strong but insignificant warming of 0.2–0.4 °C was concentrated in the Caspian Sea and Aral Sea, probably because of the internal variability of the model. A significant ($p < 0.05$) warming of 0.2–0.7 °C was mostly detected in Southeast China, India and mainland Southeast Asia (Figure 2(a)). Overall, LUCC decreased the mean T_{max} over the majority of the Eurasian continent, with significant ($p < 0.05$) cooling (approximately −0.7 to −0.4 °C) observed in Southeast and Northeast China and Europe (Figure 2(b)). These findings indicate that significant changes in the mean T_{min} and T_{max} appeared in regions with intensive LUCC (Figure 1(d)), which agrees with previous studies (Hua and Chen, 2013b; Xu *et al.*, 2015). Interestingly, LUCC in central and eastern China led to an increase in T_{min} but a decrease in T_{max} (Figure 2). The possible mechanism of these different responses of T_{min} and T_{max} to LUCC will be elucidated in Section 4.2.

3.2. Effects of LUCC on the absolute temperature indices

Figure 3 depicts the effects of LUCC on the annual mean TNn (Figure 3(a)), TNx (Figure 3(b)), TXn (Figure 3(c)) and TXx (Figure 3(d)) over Eurasia. Compared to the mean T_{max} changes (Figure 2(b) *vs* Figures 3(c) and (d)), the responses of TXx and TXn to LUCC had similar spatial distributions, with cooling over most area of Eurasian continent and significant changes in Southeast and Northeast China and Europe. The LUCC-induced changes in TNx and TNn were generally consistent with the spatial patterns of the mean T_{min} difference (Figures 3(a) and (b) *vs* Figure 2(a)). In detail, the area to the north of 50°N broadly showed insignificant cooling in TNx and TNn, while most of the area to the south of 50°N experienced warming, particularly in Southeast China, India and mainland Southeast Asia, which saw significant increases of 0.2–0.7 °C. Despite the similar spatial distributions of the LUCC-induced changes in these temperature indices, different responses in the magnitudes evidently existed. For instance, compared to the mean T_{max}, the significant decrease in TXx (approximately −1 °C) was larger in western Siberia, Europe, and Northeast and Southeast China (Figure 3(c)), while smaller decreases in TXn occurred over eastern China and western Siberia (Figure 3(d)). The LUCC-induced changes in the T_{max} indices (i.e., TXn and TXx) were generally consistent with Pitman *et al.* (2012), but more robust results of T_{min} indices (i.e., TNn and TNx) have been detected over the

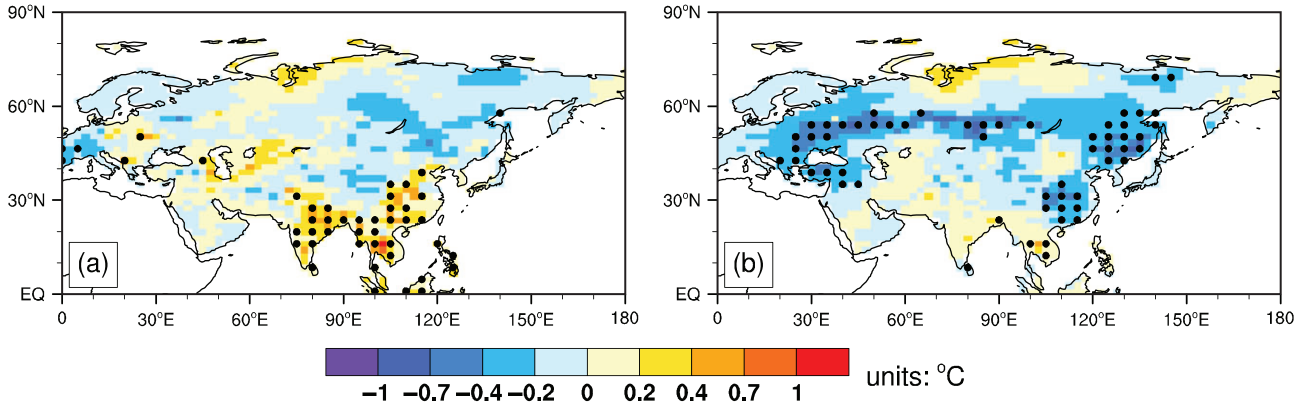

Figure 2. Simulated annual mean change of (a) minimum air temperature, and (b) maximum air temperature due to LUCC. Solid black dots denote regions where the differences are statistically significant at 95% confidence level.

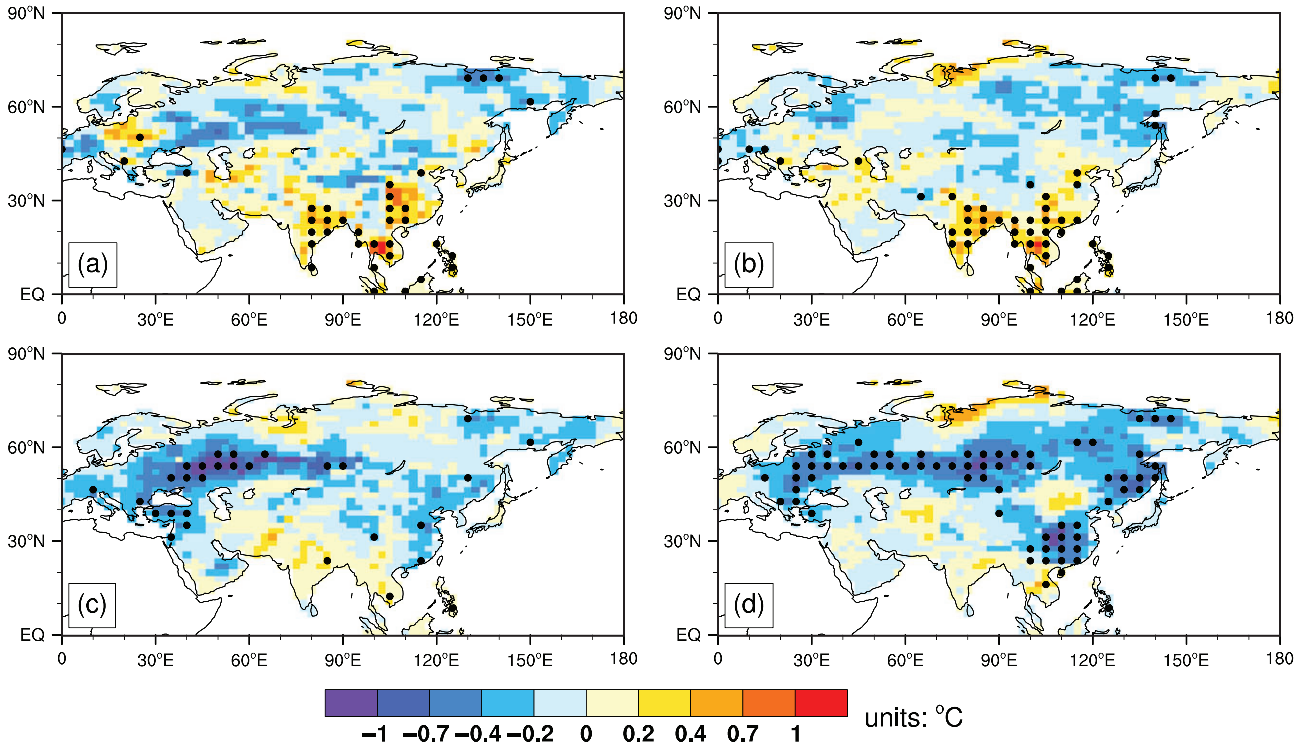

Figure 3. Same as Figure. 2 but for (a) TNn, (b)TNx, (c)TXn, (d)TXx, respectively. Solid black dots denote regions where the differences are statistically significant at 95% confidence level.

mid-to-low latitudes in our study. Christidis *et al.* (2013) found that global mean LUCC signals can be detected in warm but not cold extremes, which also agreed with our findings. In summary, the similar detected spatial patterns between the mean and extreme states probably suggest that variations in the absolute temperature indices were closely linked to LUCC-induced mean T_{min} and T_{max} changes.

3.3. Effects of LUCC on the percentile-based temperature indices

The effects of LUCC on annual percentile-based temperature indices (i.e., TN10P, TN90P, TX10P and TX90P) are shown in Figure 4. LUCC broadly reduced the number of cold nights (TN10P, Figure 4(a)) and warm nights (TN90P, Figure 4(b)) over the area to the north of 30°N. However, opposite responses to LUCC were detected to the south of 30°N, particularly in Southeast China, India and mainland Southeast Asia, each of which exhibited significant ($p < 0.05$) changes. In detail, the number of cold nights decreased by approximately 10 days in these aforementioned regions, but the number of warm nights increased by approximately 10 days. Combined with the above analyses of TNx (Figure 3(a)) and TNn changes (Figure 3(b)), the responses of the T_{min} extremes to LUCC were symmetrical [i.e., same patterns and magnitudes in both TNn (TN10P) and TNx (TN90P)], which was possibly caused by changes in the mean state of T_{min}. LUCC-induced changes in cold days (TX10P) experienced increasing in most of the area between 30° and 60°N, while decreasing

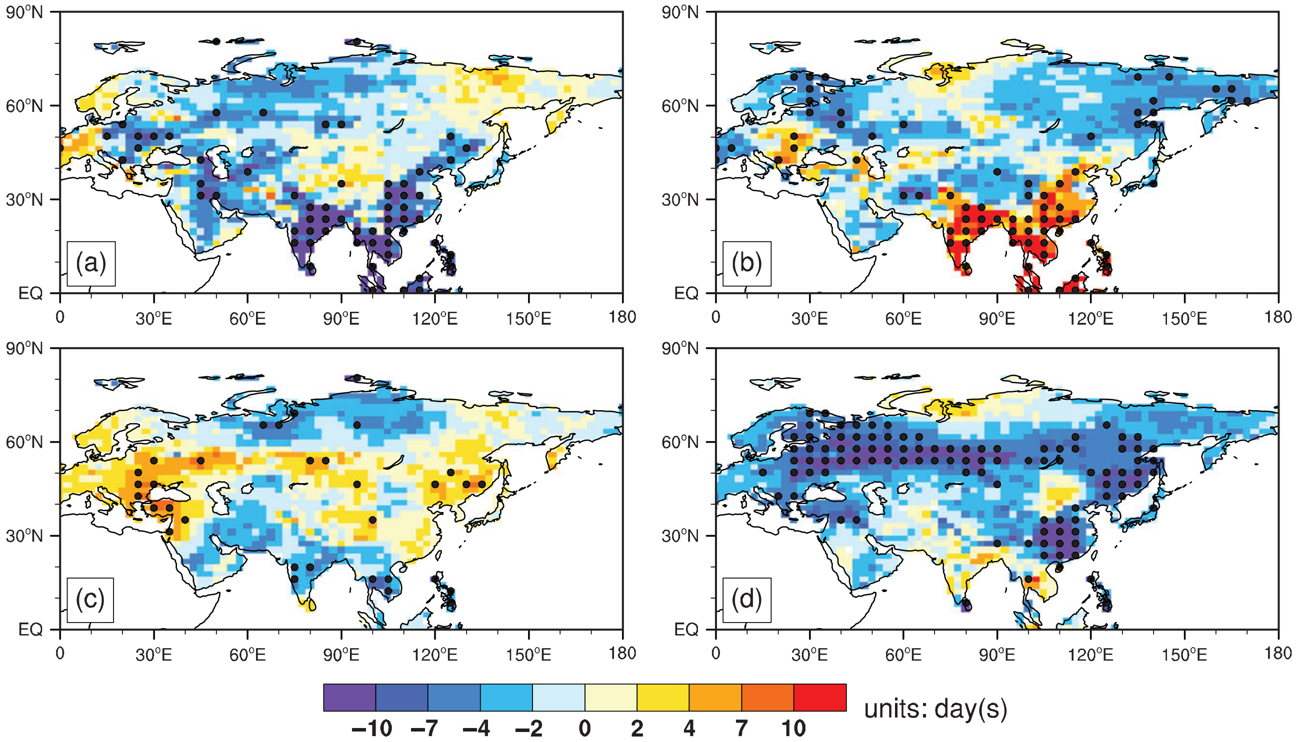

Figure 4. Same as Figure 2 but for (a) cold nights (TN10P), (b) warm nights (TN90P), (c) cold days (TX10P), (d) warm days (TX90P), respectively. Solid black dots denote regions where the differences are statistically significant at 95% confidence level.

in other regions of Eurasia (Figure 4(c)). However, significant ($p < 0.05$) changes were detected in only a few areas, i.e., in Eastern Europe and Northeast Asia (+4 days) and in India and mainland Southeast Asia (approximately −7 to −4 days). As depicted in Figure 4(d), LUCC greatly decreased the number of warm days (TX90P) over the study region; in particular, Southeast China, Northeast Asia, western Siberia and Eastern Europe saw significant ($p < 0.05$) decreases of more than 10 days. These larger changes in TX90P (TXx) compared to TX10P (TXn) imply that the T_{max} indices exhibited changes beyond the mean because of LUCC, which was probably linked to changes in the variance and/or SPD (i.e., non-mean-state) of T_{max}. In addition, we calculated the effects of LUCC on other temperature indices [i.e., threshold (SU, TR, FD and ID; definitions can be found in Table 1) and duration indices (CSDI, WSDI and GSL)]. Details can be found in the Figures S5 and S6 (Supporting information).

3.4. Relative contributions of changes in the mean state and non-mean-state on temperature extremes

The above results suggest that T_{min} extremes were probably influenced by changes in the mean state, while T_{max} extremes were very likely linked to changes in both the mean state and non-mean-state (i.e., variance and SPD). In this section, we further examine the relative contributions of the two factors (i.e., changes in mean state and non-mean-state) to the changes in temperature extremes by using the thresholds (i.e., 10^{th} and 90^{th} percentile) and mean state of daily T_{max}/T_{min}. As temperature generally follows a normal distribution, the difference between the thresholds and mean state of T_{max}/T_{min} (DTMT) can roughly measure the changes in the non-mean-state of T_{max}/T_{min}. DTMT equals zero if the probability density function shifts to the warmer or colder side without changes in non-mean-state. In contrast, DTMT may deviate from zero if there is a change in symmetry (i.e., SPD) or variability (i.e., variance).

Figure 5 shows LUCC impacts on the annual mean 10th (Figure 5(a)) and 90th (Figure 5(b)) percentiles of T_{max} and the differences from changes in mean T_{max} [i.e., 10th minus the mean (Figure 5(c)) and 90th minus the mean (Figure 5d)]. The similar spatial patterns in Figure 5 and the previous results (i.e., Figures 3 and 4) imply that the T_{max} extremes were largely associated with changes in the 10th and 90th percentiles of T_{max}. In detail, LUCC broadly cooled the 90th percentile of T_{max} over most of the continent, with significant ($p < 0.05$) changes of more than −0.4 °C over EUWS, CAEC and Northeast Asia (Figure 5(b)). However, the responses of the 10th percentile of T_{max} were much weaker than those of the 90th percentile (Figure 5(a)). The 10^{th} percentile of T_{max} still exhibited a cooling response to LUCC over EUWS, CAEC and Northeast Asia but with smaller magnitudes and confidence levels over these regions (e.g., approximately −0.2 to −0.4 °C in EUWS and Northeast Asia and approximately 0 to −0.2 °C in CAEC). Although a strong warming (cooling) response of the 10th (90th) percentile of T_{max} was located over Northeast Siberia, no significant ($p < 0.05$) changes were detected, possibly because of the remote effect of LUCC and/or the internal variability of the model. We then calculated the responses of

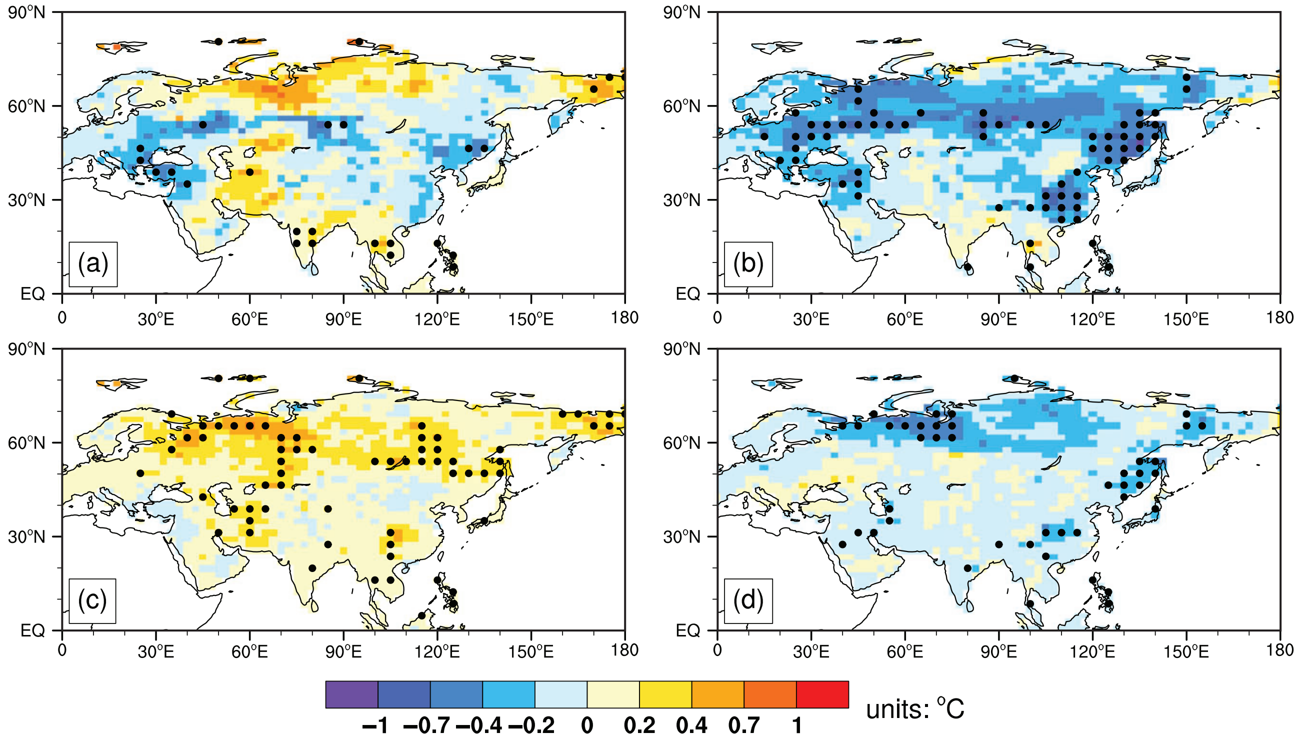

Figure 5. Simulated annual mean changes in (a) 10th and (b) 90th percentile of daily T_{max} induced by LUCC, and their corresponding results with mean state change removed [i.e. (c) 10th percentile minus mean and (d) 90th percentile minus mean]. Solid black dots denote regions where the differences are statistically significant at 95% confidence level.

the 10th and 90th percentiles of T_{max} after removing the LUCC-induced mean state changes (i.e., LUCC-induced changes in the non-mean-state of T_{max}), which could be used to quantify the relative contributions of changes in the mean state and the non-mean-state to the 10th and 90th percentiles of T_{max}. As shown in Figures 5(c) and 5(d), the responses of the 10th (90th) percentile of T_{max} to LUCC-induced changes in the non-mean-state exhibited slight warming (cooling) of 0–0.2 °C (approximately 0 to −0.2 °C) over most of the Eurasian continent. However, significant ($p < 0.05$) warming (cooling) of 0.2–0.7 °C (approximately −0.2 to −0.7 °C) was detected over CAEC, Northeast Asia and some parts of Siberia (Figures 5(c) and (d)). In addition, we have done examinations of the LUCC-induced changes in variance and skewness of T_{max}/T_{min} (See Figures S7 and S8), and found that the LUCC-induced change in variance of T_{max}/T_{min} was much bigger than that in skewness. These results implied that changes in non-mean-state on the 10th (90th) percentile of T_{max} were probably contributed by the changes in variance of T_{max}. Overall, the combined effects of changes in the mean state, the variance and/or SPD of T_{max} eventually caused the asymmetric responses of its 10th and 90th percentiles and the related extremes (e.g., TXn, TX10P, etc.).

Figure 6 shows the effects of LUCC on the annual mean 10th (Figure 6(a)) and 90th (Figure 6(b)) percentiles of T_{min} and the differences from changes in mean T_{min} (Figures 6(c) and (d)). Unlike the changes in the 10th and 90th percentiles of T_{max}, there were generally the same patterns of the changes in the 10th and 90th percentiles of T_{min} (Figures 6(a) and (b)), which were also reflected in the T_{min} extremes (i.e., Figures 3 and 4). In detail, significant ($p < 0.05$) warming of 0.4–0.7 °C occurred in both the 10th and 90th percentiles of T_{min} over most of ISEA and CAEC, while strong responses in other regions (e.g., strong warming around the Aral Sea in the 10^{th} percentile of T_{min} and strong cooling over regions to the north of 50°N in the 90th percentile of T_{min}) were insignificant. Additionally, we performed similar analyses to examine the contribution of changes in the non-mean-state of T_{min}. As shown in Figures 6(c) and (d), the effects of LUCC-induced changes in the non-mean-state caused slight warming (cooling) in the 10th (90th) percentile of T_{min} over most of Eurasia. However, strong but insignificant warming (cooling) still occurred in the 10th (90th) percentile of T_{min} over regions to the north of 50°N. Similar to T_{max}, changes in non-mean-state of T_{min} were also probably contributed by changes in variance (although the effect was relatively minor). The results indicated that the changes in the 10th and 90th percentiles of T_{min} and their corresponding extremes (i.e., TN10P, TN90P, TNn and TNx) largely depended on changes in the mean state.

Finally, we calculated the relative contributions of these two factors (i.e., changes in the mean state and non-mean-state) to the 10^{th} and 90^{th} percentiles of T_{max} and T_{min} over three sub-regions (Figure 7). The relative contribution of each factor is defined as the ratio of changes induced by one factor to the total changes (in

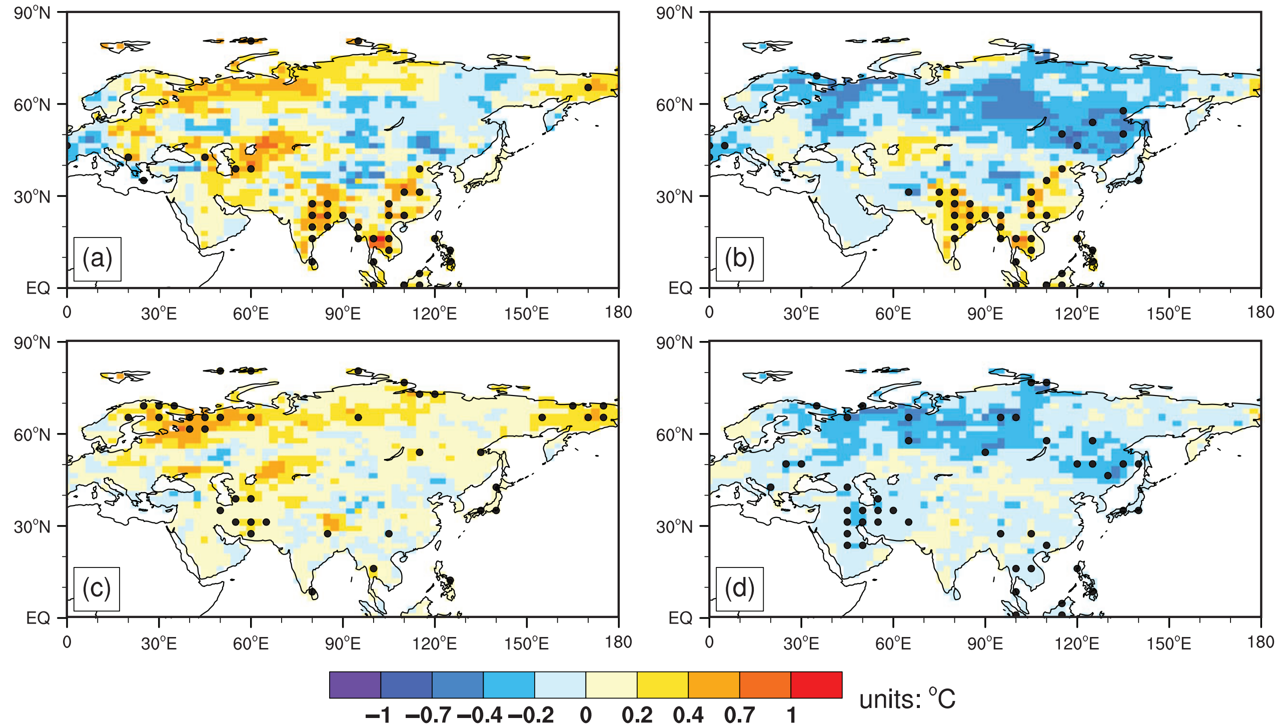

Figure 6. Same as Figure 5 but for T_{min}.

absolute value terms). More than half of the changes for T_{max} could be attributed to changes in the mean state over EUWS and CAEC (Figure 7a). However, changes in the non-mean-state also played a comparable role (i.e., the contribution was approximately 36.6%) on the changes in the 10th and 90th percentiles over CAEC. In addition, the responses to changes in the mean state and non-mean-state over ISEA were small and insignificant (Figure 7(a)). The changes for T_{min} were mostly influenced by changes in the mean state, while small contributions (approximately 10.2%) from changes in the non-mean-state were detected in the changes in the 10th and 90th percentiles over CAEC and ISEA (Figure 7(b)). Similar to the responses of T_{max} in ISEA, the contributions from changes in the mean state and non-mean-state were also very slight. Overall, the LUCC-induced changes in both the 10th and 90th percentiles of T_{max} and T_{min} and their related extreme indices mainly depended on shifts in the LUCC-induced mean state. In the next section, we will focus on the characteristics and mechanisms of LUCC-induced changes in the mean state of T_{max} and T_{min}.

4. Discussion

Our results suggested LUCC could significantly affect temperature extremes. Moreover, we also found that LUCC-induced changes in temperature extremes are largely dominated by shifts in the mean state of T_{max} and T_{min}. Thus, discussing the possible mechanisms on LUCC-induced changes in mean T_{min} and T_{max} is a bridge of comprehending how temperature extremes respond to LUCC. In the following, we would like to perform further investigations on mean T_{min} and T_{max} changes due to LUCC in terms of two major questions: (1) whether (see Section 4.1) and ((A.1)) why (see Sections 4.2 and 4.3)

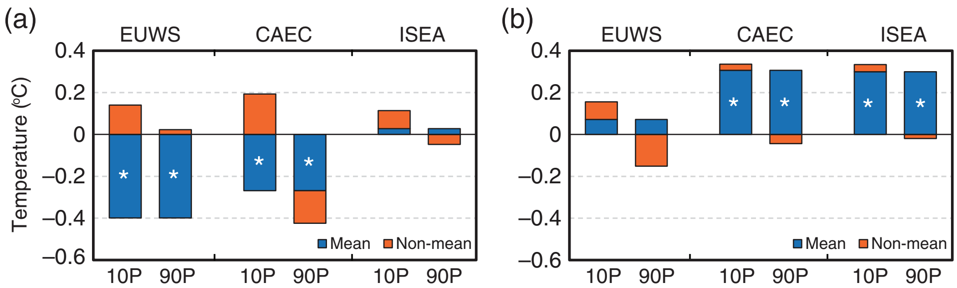

Figure 7. The relative contribution of changes in mean state (blue) and non-mean-state (i.e., variance and/or shape of probability distribution) (orange) to the changes in 10th (10P) and 90th percentile (90P) of daily (a) T_{max} and (b) T_{min} over sub-regions. A white asterisk in the middle of the bar represents the value is statistically significant at 95% confidence level.

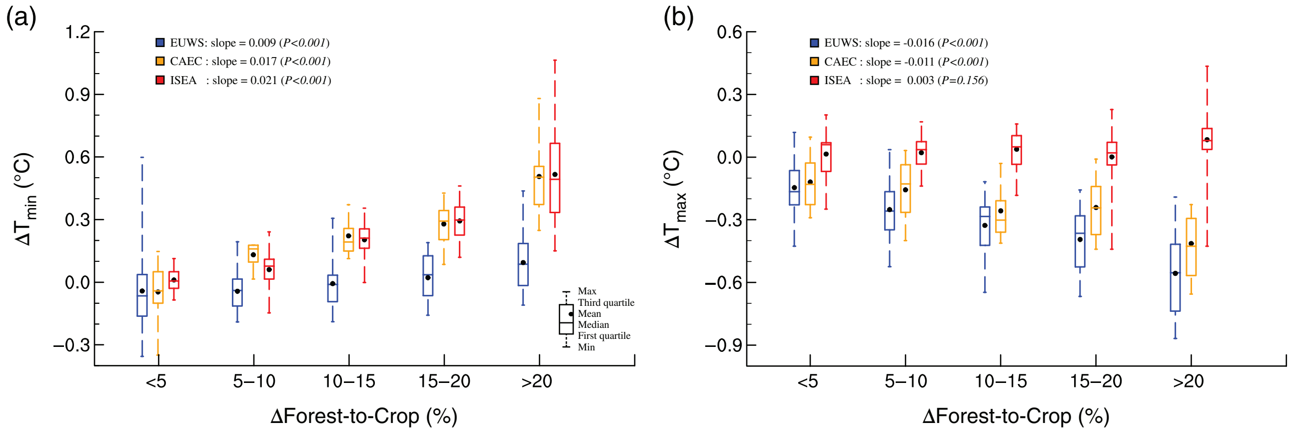

Figure 8. Box-and-Whisker plot of forest-to-crop changes and (a) changes in T_{min}, (b) changes in T_{max} over three regions. The regression slopes (units: °C/1% forest-to-crop change) of forest-to-crop change and temperature over regions are also shown in each plot, only grid points where percentage of forest-to-crop change over 10% were included in calculation.

spatial differences exist in T_{min} and T_{max} responses (i.e., magnitude) to LUCC.

4.1. Differences in the sensitivities of T_{min} and T_{max} to LUCC

To explore whether the responses of T_{min} and T_{max} to LUCC differ among regions, three typical areas with robust changes from forests to crops were selected (Figure 1(d)). The relationship between LUCC and changes in T_{min} and T_{max} in each region was then quantified. Herein, the quantifiable LUCC is defined as the conversion from forests to crops [($\Delta crop$ − $\Delta forest$)/2]. Obviously, the larger the forest-to-crop changes are, the larger the positive anomalies from LUCC become for a given mean T_{min} in each selected region (Figure 8(a)). Note that in the regions with forest-to-crop change lower than 10%, the LUCC-induced changes in T_{min} and T_{max} are rather weak and insignificant. Therefore, we consider all grids with forest-to-crop changes that are above 10% to estimate the sensitivity of T_{max} and T_{min} to LUCC, which can be represented by the linear regression coefficient (i.e., slope) for each selected region. The responses of T_{min} to LUCC for each region were all positive, and the magnitudes increased with increasing forest-to-crop changes. However, the T_{min}'s sensitivity to LUCC exhibited obvious differences between regions (Figure 8(a)). For example, ISEA had the largest sensitivity to each unit of forest-to-crop change (0.021 °C), followed by CAEC and EUWS, which had slopes of 0.017 and 0.009 °C, respectively. For T_{max}, the magnitudes of the LUCC-induced negative anomalies over EUWS and CAEC increased with increasing forest-to-crop changes, while ISEA showed a slight increase in its positive anomalies (Figure 8(b)). Moreover, the T_{max}'s sensitivity to LUCC was also regionally dependent. In detail, the sensitivity to each unit of forest-to-crop change was significantly ($p < 0.05$) negative over EUWS (−0.016 °C) and CAEC (−0.011 °C) but insignificantly positive over ISEA (0.003 °C).

4.2. Possible mechanism of region-specific LUCC-induced T_{min} and T_{max} responses

LUCC can influence the surface energy balance by modifying the physical properties (e.g., albedo and surface roughness) of the land surface and consequently affect the temperature (Boisier *et al.*, 2012). To explore the mechanisms of regional differences in the sensitivity of T_{min} and T_{max} to LUCC, we introduce a decomposed temperature metric (DTM) to estimate the contributions of each surface energy component (i.e., solar radiation that is absorbed by the land surface, SR_{net}; downward atmospheric long-wave radiation, LR_{down}; upward long-wave radiation from the land surface, LR_{up}; sensible heat flux, SH; latent heat flux, LH; and ground heat flux, G), each of which has a temporal resolution of three hours. Detailed information regarding the computational formulas is shown in the Appendix. Figure 9 shows the sensitivity of the daytime and nighttime surface radiative temperature to LUCC-induced surface energy components (see Equations ((A.1))–(A.(A.5)) in the Appendix). For a convenient comparison, S_{SH}, S_{LH} and S_G are multiplied by −1.

During the daytime, the summarized temperature tendency to each energy component showed significant ($p < 0.05$) decreases in both CAEC (−0.007 °C per 1% forest-to-crop change; the units of temperature sensitivity or tendency are hereinafter referred to as '°C/FCC') and EUWS (−0.012 °C/FCC; Figure 9(a)). Changes in SR_{net}, which mainly resulted from LUCC-induced albedo changes, induced an almost identical decrease in the temperature tendency over CAEC (−0.034 °C/FCC) and EUWS (−0.036 °C/FCC). The LR_{down}-induced changes in the temperature tendency exhibited slight decreases in CAEC (−0.001 °C/FCC) and EUWS (−0.011 °C/FCC). The reduction of SR_{net} and LR_{down} directly reduced the amount of available radiative energy at the land surface, which tended to cool the land surface. On the other hand, LUCC also led to a significant change in the partitioning of the non-radiative terms (e.g., SH, LH and G; Bright, 2015). For example, SH significantly decreased in the CAEC and EUWS regions in daytime presumably due

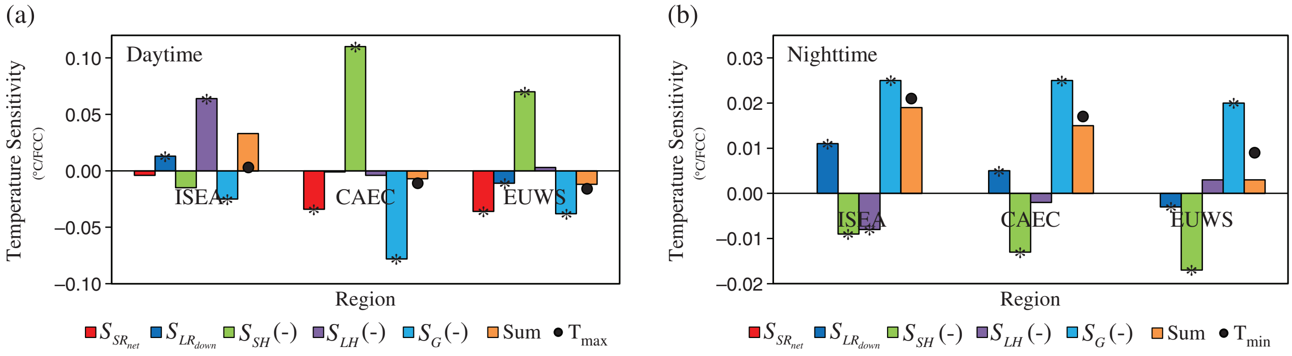

Figure 9. LUCC-induced temperature sensitivity derived from changes in various components of surface energy budget in (a) daytime and (b) nighttime over three sub-regions, units: °C/1% forest-to-crop change, referred to as '°C/FCC'. Bars indicate the sensitivity of surface temperature induced by that of absorbed solar radiation (red), downward atmospheric long-wave radiation (dark blue), sensible heat flux (green), latent hear flux (purple), ground heat flux (light blue) to LUCC and the computed net surface temperature sensitivity (sum of all components, orange). For a convenient comparison, S_{SH}, S_{LH} and S_G are multiplied by −1. Solid black dots indicated that the simulated sensitivity of $T_{\max}$ and $T_{\min}$ to LUCC. An asterisk on the bar represents the slope is statistically significant at 95% confidence level. Note that Daytime (nighttime) is set to UTC 06 (UTC 18) for CAEC, UTC 09 (UTC 21) for ISEA and UTC 12 (UTC 00) for EUWS.

to the reduced land surface roughness (Zhang, *et al.*, 2016). Consequently, the daytime land surface temperature tendency increased by 0.11 °C/FCC (0.07 °C/FCC) in the CAEC (EUWS) in response to the change in SH (Figure 9(a)). G showed a similar change as SH but with a different sign. An increase in G suggests that the residue of the turbulent heat fluxes (i.e., SH and LH) is transmitted and stored in deep soil, which caused the temperature tendency to decrease by −0.078 °C/FCC (−0.038 °C/FCC) in CAEC (EUWS; Figure 9(a)). In contrast, LUCC-induced changes in LH were relatively weak and insignificant in the CAEC and EUWS regions, consequently resulting in the temperature tendency to decrease (increase) by −0.004 °C/FCC (0.003 °C/FCC) in CAEC (EUWS; Figure 9(a)). Finally, the warming effects of SH were offset by the cooling effects of G, which induced small changes in $T_{\max}$ in both CAEC and EUWS. However, different from CAEC and EUWS, the decrease in SR_{net} in ISEA was much smaller (−0.004 °C/FCC). The LR_{down}-induced temperature tendency increased by a small magnitude (0.013 °C/FCC). Furthermore, the partition of non-radiative fluxes was mostly concentrated in a dampened LH, which increased the surface temperature. In addition, higher SH and G-induced identical cooling effects, which cancelled out some of the LH-induced warming. Thus, the temperature tendency in ISEA eventually increased.

During the nighttime, SR_{net} decreased to zero, and the other terms of the energy components determined $T_{\min}$. Generally, the sum of the surface temperature tendency that was induced by each energy component exhibited a significant ($p < 0.05$) increase over CAEC (0.015 °C/FCC) and ISEA (0.019 °C/FCC) but an insignificant increase over EUWS (0.003 °C/FCC). The greater amount of G that was stored by deep soil during the daytime travelled upward to the surface at night, which dominated the increase in surface temperature over these three regions. As shown in Figure 9, the positive (negative) G responses during the daytime (nighttime) suggest that the diurnal cycle of G was significantly enhanced because of LUCC. This effect has been long noted and offered as the primary mechanism of LUCC-induced DTR reduction in previous studies (Oke, 1978; Rosenberg *et al.*, 1983). However, the diurnal cycle of SH was dampened [because of the dampened upward (downward) SH during the daytime (nighttime); Figure 9], which tended to warm the surface during the daytime and cool the surface during the nighttime. In addition, the small changes in temperature tendencies that were induced by LR_{down} and LH at night cancelled each other out over these three regions, despite the different signs between ISEA/CAEC and EUWS. Finally, smaller SH-induced cooling with greater G-induced warming-induced significant warming over ISEA and CAEC, while the SH and G over EUWS almost completely offset each other, creating a slight response in temperature tendency.

In summary, the effect of LUCC on the albedo significantly decreased the SR_{net} during the daytime and directly cooled the $T_{\max}$. Mutual inhibition from SH and G played an equivalently important role in determining $T_{\max}$ and $T_{\min}$ over the regions with strong LUCC-induced responses (i.e., EUWS and CAEC during the daytime and ISEA and CAEC during the nighttime). In contrast to the simulated $T_{\max}$ and $T_{\min}$ sensitivity, the DTM could explain 63.6% of the $T_{\max}$'s sensitivity to LUCC in CAEC and 75% of that in EUWS (Figure 9(a)), along with 90.5% and 88.2% of the $T_{\min}$'s sensitivity in ISEA and CAEC, respectively (Figure 9(b)). However, the DTM seemed to deviate in its interpretation of the changes in $T_{\max}$ and $T_{\min}$ over regions with insignificant responses (i.e., ISEA during the daytime and EUWS during the nighttime), which possibly originated from three aspects: (1) the 3-hourly temporal resolution of the selected energy components, which were used to diagnose the possible mechanism of temperature sensitivity, was coarse, and even their corresponding times may have mismatched with the occurrence times of the daily $T_{\min}$ ($T_{\max}$); (2) changes in the surface emissivity, which should have been contained in the original DTM, were ignored in this study; and (3) the simulated

Table 2. The climatology of various energy components (units: W m^{-2}) among sub-regions at daytime.

LU1850	SR_{net}	LR_{down}	LR_{up}	SH	LH	G	Bowen ratio
EUWS	294.013	308.935	383.787	96.286	74.575	48.300	1.291
CAEC	458.424	352.900	433.279	143.407	144.615	90.023	0.991
ISEA	495.779	404.527	493.574	136.085	191.785	78.862	0.710
LU2000							
EUWS	288.785	308.002	382.475	89.341	74.525	50.446	1.199
CAEC	452.603	352.852	432.179	129.246	145.051	98.979	0.891
ISEA	496.831	404.892	497.244	133.574	186.582	84.323	0.716

T_{max} and T_{min} are 2-m air temperature, which are approximate but more or less different with land surface temperatures in DTM. These shortcomings would introduce some uncertainties. Despite that, the remarkable divergences in the surface energy components across regions could adequately interpret differences in the sensitivity of T_{max} and T_{min} to LUCC. In the next section, we will discuss the possible reasons of the region-specific responses of some energy components to LUCC.

4.3. Region-specific responses for some energy components to LUCC

Numerous studies have stated that deforestation would cause a cooling effect in the mean temperature at mid-to-high latitudes but a warming effect in tropical regions (Claussen *et al.*, 2001; Bala *et al.*, 2007; Betts, 2011). Different dominant bio-geophysical processes determine this phenomenon. For instance, deforestation at mid-to-high latitudes leads to a higher albedo, which tends to reduce the incoming shortwave radiation at the surface and thus exerts a cooling effect on the surface temperature (Feddema *et al.*, 2005; Brovkin *et al.*, 2006; Bala *et al.*, 2007; Bonan, 2008; Zhang *et al.*, 2009; Devaraju *et al.*, 2011). However, reduced evapotranspiration is the main factor that warms the surface in tropical regions (DeFries *et al.* 2004; Feddema *et al.*, 2005). In our study, the significant cooling in T_{max} over mid-to-high-latitude regions (i.e., EUWS and CAEC) and the corresponding albedo-dominant mechanism were detected, which are consistent with previous findings. Two major differences existed among the regions during the daytime: (1) the differences in responses magnitude between mid- (i.e., CAEC) and high-latitude (i.e., EUWS) regions, and (2) the distinctly opposite responses between tropical regions (i.e., ISEA) and temperate regions (i.e., CAEC/EUWS). The first difference can be interpreted by the region-specific climatology of the surface energy budget, which has been showed in Table 2. The results suggest that similar LUCC (both type and intensity) over EUWS and CAEC induced consistent effects on the albedo, which is directly reflected in the identical reduction in SR_{net} (approximately -6 W m^{-2}). Besides, the partition of turbulence heat fluxes (i.e., SH and LH) was also changed by LUCC over EUWS and CAEC, which have similar decreases in Bowen ratio (approximately -0.1). However, identical changes in the Bowen ratio would cause more SH loss over CAEC (approximately -14 W m^{-2}) than EUWS (approximately -7 W m^{-2}) because of the different climatology levels of SH (i.e., EUWS: 96.29 W m^{-2}, CAEC: 143.407 W m^{-2}). Then, this discrepancy in SH was eventually transformed and stored as different G. The second difference – different responses between EUWS/CAEC and ISEA – can be explained by the different types of deforestation. As shown in Figure 10, needle-leaf evergreen trees (NET) and temperate broadleaf deciduous trees (BDT) prevails over EUWS and CAEC, while tropical BDT covered most of ISEA. According to the different PFT optical properties (e.g., albedo) that were described in Oleson *et al.* (2010) and Bonan (2002), the albedos of NET are smaller, while those of BDT are higher and close to that of grasslands/croplands (Table 3.1 in Oleson *et al.*, 2010; Table 8.1 in Bonan, 2002). Thus, deforestation over tropical regions (i.e., ISEA) would result in a slight decrease in SR_{net} (Figure 8(a)). In addition, it is noted that deforestation over tropical regions could also reduce the leaf area index (LAI) and decrease the root zone depth, which directly caused substantial losses in canopy water transpiration (Harrison and Hester, 2014). Thus, LH over ISEA significantly decreased (Fig. 9a). The evapotranspiration mechanism seemed to be less effective in the mid-to-high-latitude regions (e.g., EUWS/CAEC), probably because the albedo-induced cooling effect in the mid-to-high-latitude areas would be five times larger than the evapotranspiration-induced warming effect (Davin and de Noblet-Ducoudré, 2010). During the nighttime, the discrepancies in T_{min} across regions were mostly caused by differences in SH and G. For G, its regional differences generated in the daytime will be persist to nighttime, and partly contribute to the different responses (i.e., magnitude) of T_{min} through the warming effects of the released G from deep soil to land surface. Furthermore, different changes in the Bowen ratio and different climatology levels of SH (Table 3) were responsible for the distinct SH responses among the regions. In addition, Lee *et al.* (2011) hypothesized that the warmer nighttime temperatures in forests can be attributed to the presence of tall trees, which could enhance turbulence and thus bring heat from aloft to the surface, in contrast to open lands. Zhang *et al.* (2014) further found that this effect is stronger in the boreal zone (>45°N) but absent at low latitudes. Obviously, these findings above indicated that deforestation would probably induce more SH responses in the boreal zone than in tropical regions at night, which basically agrees with our results.

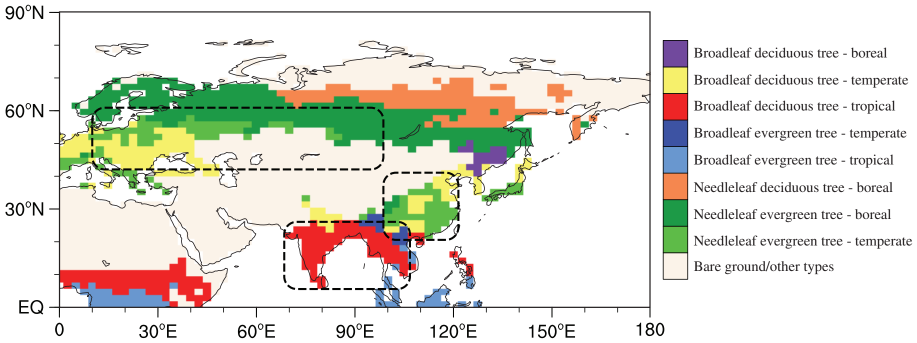

Figure 10. Primary tree cover map prescribed in LU1850; for clarity, these are grouped here according to the dominant tree type in a non-bare ground grid.

Table 3. Same as Table 2 but at nighttime (units: W m^{-2}).

LU1850	SR_{net}	LR_{down}	LR_{up}	SH	LH	G	Bowen ratio
EUWS	0	290.628	331.230	−14.560	4.519	−30.561	−3.222
CAEC	0	339.847	378.076	−9.485	7.830	−36.575	−1.211
ISEA	0	383.747	423.751	−9.921	9.311	−39.395	−1.065
LU2000							
EUWS	0	290.577	330.993	−13.197	4.323	−31.541	−3.053
CAEC	0	340.380	379.467	−7.906	8.028	−39.210	−0.985
ISEA	0	383.781	425.271	−8.956	9.666	−42.200	−0.926

In this study, we only discussed the mechanism of LUCC-induced changes in temperature extremes from the mean state change perspective; however, the mechanism of LUCC-induced changes in the non-mean-state (i.e., variance or SPD) of T_{min} and T_{max} are far more complicated and equally important (Seneviratne *et al.*, 2012; Davin *et al.*, 2014; Wilhelm *et al.*, 2015). For example, Davin *et al.* (2014) stated that summer cooling because of increases in cropland albedo is strongly amplified over the European continent during hot summer days (clear-sky conditions) but is counteracted by a negative cloud feedback mechanism during cloudy days. Wilhelm *et al.* (2015) extended this work by using a fully coupled Earth system model (CESM) and investigated albedo-induced asymmetric changes in temperature extremes in the recent past and the future. These works provided a possible physical explanation on how LUCC affects the asymmetric response of temperature extremes.

5. Conclusions

Extensive evidence demonstrated that LUCC exerts more prominent effects on extreme temperature than mean temperature. Firstly, we quantified the potential effects of LUCC over Eurasia on temperature extremes (i.e., percentile-based temperature indices, absolute temperature indices, and others) by idealized numerical experiments that were based on NCAR CAM5 coupled with CLM4. The historical LUCC over Eurasia was generally dominated by deforestation and cropland expansion, especially in the selected regions (i.e., some parts of ISEA, CAEC and most of EUWS), where forest-to-crop changes was higher than 20%. Generally, LUCC-induced changes in temperature extremes were robust in the study regions. LUCC-induced significant ($p < 0.05$) warming (0.2–0.7 °C) in the mean T_{min} in ISEA and CAEC, followed by symmetrical warming in TNx and TNn and a decrease (increase) in TN10P (TN90P). For the mean T_{max}, LUCC-induced broad and significant ($p < 0.05$) cooling (−0.7 °C ∼ −0.4). Its high-percentile indices exhibited obvious responses over CAEC and EUWS, e.g., TXx and TX90P, which showed significant ($p < 0.05$) cooling (approximately −0.4 to −1.0 °C) and decreases (higher than 10 days), respectively, but its low-percentile indices (i.e., TXn and TX10P) exhibited relatively weak responses over the same regions. Furthermore, we confirmed that the changes in T_{min} extremes were mostly influenced by changes in the mean state of temperature (approximately 90%), while changes in both the mean state (approximately 63.4%) and SPD (approximately 36.6%) contributed to changes in T_{max} extremes. In addition, the responses of temperature extremes to LUCC exhibited evident regional features.

Furthermore, the characteristics and possible mechanisms of LUCC-induced changes in the temperature extremes over these three regions (i.e., EUWS, ISEA and CAEC) were discussed in terms of changes in the mean state of T_{min} and T_{max}. Analyses indicated that the mean T_{min} and T_{max} in certain regions with more robust LUCC exhibited larger temperature anomalies, but their responses also exhibited evident regional features. Moreover, these region-specific responses mainly resulted from the different sensitivity of T_{min} and T_{max} to LUCC across these three regions. For example, the strongest warming (cooling) effect on the sensitivity of T_{min} (T_{max}) to LUCC was detected in ISEA (EUWS) compared to the other two regions. By introducing the decomposed temperature metric, we found that the T_{max}'s sensitivity in EUWS and CAEC was mainly controlled by SR_{net}, SH and G, while the T_{min}'s sensitivity was determined by G and SH during the nighttime. Briefly, LUCC-induced changes in the energy flux component could explain approximately 70 and 90% of the changes in the sensitivity of T_{max} and T_{min}, which implies that changes in these energy flux components determined the spatial differences in the sensitivity of T_{min} and T_{max} to LUCC. In addition, we discussed the possible causes of the distinct responses of the energy components among the regions and found that the climatology value of the energy components and the dominant plant functional types were responsible.

Although the current results seemed to be robust, some uncertainties still exist that should be clarified. First, a single model simulation with limited ensemble members would cause any related conclusions to become model dependent and introduce some uncertainties in particular for analyses of extreme values. Hence, multi-model simulations with sufficient ensemble runs would allow us to derive more robust and confident results. Second, considering a single LUCC scenario (i.e., the Land-Use Harmonization dataset from Hurtt *et al.*, 2011) would also make the results data dependent. However, many reconstruction datasets of historical land use/land cover are also available (e.g., Ramankutty and Foley, 1999; Pongratz *et al.*, 2008; Goldewijk *et al.*, 2010, 2011), so multi-scenario simulations should also be considered in future studies. Third, the ocean variability and air-sea feedback, which might also potentially affect temperature extremes, was omitted. As reported by Ma *et al.* (2013), the hydrologic cycle and moisture conditions are largely amplified over East China when including ocean variability in an afforestation experiment, which implies that the related mechanisms would be completely different.

Despite this study's incompleteness, we provided some clues and insights into the effects of LUCC on temperature extremes and provided implications for possible explanations of region-specific responses to LUCC. In a future work, we will focus on the perspective of quantile variations in temperature extremes.

Acknowledgements

This study was jointly supported by the National Natural Science Foundation of China (Grant Nos. 41475083, 41625019, 41605034), the Special Fund for Research in the Public Interest of China (Grant No. GYHY201406020), the Natural Science Foundation of Jiangsu Province, China (Grant Nos. BK20160948, BK20151525), Project Funded by the Priority Academic Program Development of Jiangsu Higher Education Institutions (PAPD), the Natural Science Foundation for Higher Education Institutions in Jiangsu Province (16KJB170007) and the Innovation Research Program for College Graduates of Jiangsu Province (Grant No. KYZZ15_0243). We are particularly indebted to two anonymous reviewers for their painstaking and highly valuable suggestions for improvements to the manuscript.

Appendix: Decomposition of surface temperature changes

Here, the surface energy balance equation is expressed as:

$$\mathrm{SR_{net}} + \mathrm{LR_{down}} - \mathrm{LR_{up}} - \mathrm{SH} - \mathrm{LH} - G = 0 \qquad ((\mathrm{A.1}))$$

Based on the Stefan–Boltzmann law, the surface upward long-wave radiation in Equation ((A.1)) can be approximated by using first-order Taylor series expansion with T_{rs_1850}:

$$T^4_{rs\_2000} = T^4_{rs\_1850} + 4T^3_{rs\_1850}\left(T_{rs\_2000} - T_{rs\_1850}\right) \qquad ((\mathrm{A.2}))$$

Then, the surface radiative temperature change ($\Delta T_{rs} = T_{rs\_2000} - T_{rs\_1850}$) can be computed as follows:

$$\Delta T_{rs} = \frac{1}{4}\sigma^{-\frac{1}{4}} \cdot \mathrm{LR}_{\mathrm{up}_{1850}}^{-\frac{3}{4}} \cdot \Delta\mathrm{LR_{up}} \qquad ((\mathrm{A.3}))$$

where σ is the Stefan–Boltzmann constant, which equals 5.671×10^{-8} W/(m^2 K^4), and ΔLR_{up} ($\Delta LR_{up} = LR_{up\_2000} - LR_{up\_1850}$) denotes LUCC-induced changes in upward long-wave radiation. In addition, the surface emissivity is set to 1.0.

The changes in SR_{net}, LR_{down}, SH, LH, and G (expressed as ΔSR_{net}, ΔLR_{down}, ΔSH, ΔLH and ΔG; all the changes are calculated as LU2000 minus LU1850) can also be expressed as an upward infrared radiation anomaly (ΔLR_{up}):

$$\Delta\mathrm{LR_{up}} = \Delta\mathrm{SR_{net}} + \Delta\mathrm{LR_{down}} - \Delta\mathrm{SH} - \Delta\mathrm{LH} - \Delta G \qquad ((\mathrm{A.4}))$$

Based on Equations ((A.3)) and ((A.4)), we can determine which component(s) of the energy budget is responsible for the changes in the T_{max} (T_{min}) by analysing changes in the surface energy fluxes at daytime (nighttime). Daytime (nighttime) is set to UTC 06 (UTC 18) for CAEC, UTC 09 (UTC 21) for ISEA and UTC 12 (UTC 00) for EUWS. This decomposition method was proposed by Juang *et al.* (2007) and has been widely used to attribute LUCC-induced temperature changes to surface energy components (Boisier *et al.*, 2012; Luyssaert *et al.*, 2014; Xu *et al.*, 2015; Chen and Dirmeyer, 2016).

Furthermore, the sensitivity (all the sensitivity calculations only consider grid points with more than 10% forest-to-crop changes) of ΔT_{rs} ($S_{T_{rs}}$) to LUCC (expressed as the same definition in Section 4.1) can be calculated as the linear regression coefficient (i.e., slope):

$$S_{T_{rs}} = \mathrm{d}T_{rs}/\mathrm{dLUCC} \qquad ((\mathrm{A.5}))$$

By combining Equations ((A.3)), ((A.4)) and ((A.5)), the contribution of each energy flux change to LUCC-induced changes in the sensitivity of T_{min} and T_{max} over ISEA, CAEC and EUWS can be diagnosed by transforming the above equation into the following:

$$S_{T_{\mathrm{rs}}} = S_{\mathrm{SR}_{\mathrm{net}}} + S_{\mathrm{LR}_{\mathrm{down}}} - S_{\mathrm{SH}} - S_{\mathrm{LH}} - S_G \qquad ((\mathrm{A.6}))$$

Equation. ((A.6)) states that the sensitivity of $T_{\min}$ and $T_{\max}$ to LUCC is determined by five factors in the numerator: the sensitivity of the net solar radiation to LUCC ($S_{\mathrm{SR}_{\mathrm{net}}}$), the sensitivity of the downward long-wave radiation ($S_{\mathrm{LR}_{\mathrm{down}}}$), and the sensitivities of the surface latent, sensible heat and ground heat fluxes (S_{SH}, S_{LH} and S_G).

Supporting information

The following supporting information is available as part of the online article:

Appendix S1. Assessment of temperature extremes simulated by CAM5.

Appendix S2. Impact of LUCC on other temperature indices.

Appendix S3. Impact of LUCC on the variance and skewness of $T_{\max}/T_{\min}$.

References

Alexander LV, Zhang X, Peterson TC, Caesar J, Gleason B, Klein Tank AMG, Haylock M, Collins D, Trewin B, Rahimzadeh F, Tagipour A, Rupa Kumar K, Revadekar J, Griffiths G, Vincent L, Stephenson DB, Burn J, Aguilar E, Brunet M, Taylor M, New M, Zhai P, Rusticucci M, Vazquez-Aguirre JL. 2006. Global observed changes in daily climate extremes of temperature and precipitation. *J. Geophys. Res. Atmos.* **111**: D05109, doi: 10.1029/2005JD006290.

Avila FB, Pitman AJ, Donat MG, Alexander LV, Abramowitz G. 2012. Climate model simulated changes in temperature extremes due to land cover change. *J. Geophys. Res. Atmos.* **117**: D04108, doi: 10.1029/2011JD016382.

Bala G, Caldeira K, Wickett M, Phillips TJ, Lobell DB, Delire C, Mirin A. 2007. Combined climate and carbon-cycle effects of large-scale deforestation. *Proc. Natl. Acad. Sci.* **104**: 6550–6555, doi: 10.1073/pnas.0608998104.

Betts RA. 2011. Climate science: afforestation cools more or less. *Nat. Geosci.* **4**: 504–505, doi: 10.1038/ngeo1223.

Boisier JP, Noblet-Ducoudré N, Pitman AJ, Cruz FT, Delire C, Hurk BJJM, Molen MK, Müller C, Voldoire A. 2012. Attributing the impacts of land-cover changes in temperate regions on surface temperature and heat fluxes to specific causes: results from the first LUCID set of simulations. *J. Geophys. Res. Atmos.* **117**: D12116, doi: 10.1029/2011JD017106.

Bonan GB. 2002. *Ecological Climatology-Concepts and Applications*, 1st edn. Cambridge University Press: Cambridge, UK.

Bonan GB. 2008. Forests and climate change: forcings, feedbacks, and the climate benefits of forests. *Science* **320**: 1444–1449, doi: 10.1126/science.1155121.

Bounoua L, DeFries R, Collatz GJ, Sellers P, Khan H. 2002. Effects of land cover conversion on surface climate. *Clim. Change* **52**: 29–64, doi: 10.1023/A:1013051420309.

Bright RM, 2015. Metrics for biogeophysical climate forcings from land use and land cover changes and their inclusion in Life cycle assessment: a critical review. *Environ. Sci. Technol.* **49**: 3291–3303, doi: 10.1021/es505465t.

Brovkin V, Claussen M, Driesschaert E, Fichefet T, Kicklighter D, Loutre MF, Matthews HD, Ramankutty N, Schaeffer M, Sokolov A. 2006. Biogeophysical effects of historical land cover changes simulated by six Earth system models of intermediate complexity. *Clim. Dyn.* **26**: 587–600, doi: 10.1007/s00382-005-0092-6.

Chen L, Dirmeyer PA. 2016. Adapting observationally based metrics of biogeophysical feedbacks from land cover/land use change to climate modeling. *Environ. Res. Lett.* **11**: 1748–9326, doi: 10.1088/1748-9326/11/3/034002.

Christidis N, Stott PA, Brown SJ. 2011. The role of human activity in the recent warming of extremely warm daytime temperatures. *J. Clim.* **24**: 1922–1930, doi: 10.1175/2011JCLI4150.1.

Christidis N, Stott PA, Hegerl GC, Betts RA. 2013. The role of land use change in the recent warming of daily extreme temperatures. *Geophys. Res. Lett.* **40**: 589–594, doi: 10.1002/grl.50159.

Claussen M, Brovkin V, Ganopolski A. 2001. Biogeophysical versus biogeochemical feedbacks of large-scale land cover change. *Geophys. Res. Lett.* **28**: 1011–1014, doi: 10.1029/2000GL012471.

Davin EL, de Noblet-Ducoudré N. 2010. Climatic impact of global-scale deforestation: radiative versus nonradiative processes. *J. Clim.* **23**: 97–112, doi: 10.1175/2009JCLI3102.1.

Davin EL, Seneviratne SI, Ciais P, Olioso A, Wang T. 2014. Preferential cooling of hot extremes from cropland albedo management. *Proc. Natl. Acad. Sci.* **111**: 9757–9761, doi: 10.1073/pnas.1317323111.

DeFries RS, Foley JA, Asner GP. 2004. Land-use choices: balancing human needs and ecosystem function. *Front. Ecol. Environ.* **2**: 249–257, doi: 10.1890/1540-9295(2004)002[0249:LCBHNA]2.0.CO;2.

Devaraju N, Cao L, Bala G, Caldeira K, Nemani R. 2011. A model investigation of vegetation-atmosphere interactions on a millennial timescale. *Biogeosciences* **8**: 3677–3686, doi: 10.5194/bg-8-3677-2011.

Donat MG, Alexander LV, Yang H, Durre I, Vose R, Caesar J. 2013a. Global land-based datasets for monitoring climatic extremes. *Bull. Am. Meteorol. Soc.* **94**: 997–1006, doi: 10.1175/BAMS-D-12-00109.1.

Donat MG, Alexander LV, Yang H, Durre I, Vose R, Dunn RJH, Willett KM, Aguilar E, Brunet M, Caesar J, Hewitson B, Jack C, Klein Tank AMG, Kruger AC, Marengo J, Peterson TC, Renom M, Oria Rojas C, Rusticucci M, Salinger J, Elrayah AS, Sekele SS, Srivastava AK, Trewin B, Villarroel C, Vincent LA, Zhai P, Zhang X, Kitching S. 2013b. Updated analyses of temperature and precipitation extreme indices since the beginning of the twentieth century: The HadEX2 dataset. *J. Geophys. Res. Atmos.* **118**: 2098–2118, doi: 10.1002/jgrd.50150.

Dong S, Xu Y, Zhou B, Shi Y. 2015. Assessment of indices of temperature extremes simulated by multiple CMIP5 models over China. *Adv. Atmos. Sci.* **32**: 1077–1091, doi: 10.1007/s00376-015-4152-5.

Feddema J, Oleson K, Bonan G, Mearns L, Washington W, Meehl G, Nychka D. 2005. A comparison of a GCM response to historical anthropogenic land cover change and model sensitivity to uncertainty in present-day land cover representations. *Clim. Dyn.* **25**: 581–609, doi: 10.1007/s00382-005-0038-z.

Foley JA, DeFries R, Asner GP, Barford C, Bonan G, Carpenter SR, Chapin FS, Coe MT, Daily GC, Gibbs HK, Helkowski JH, Holloway T, Howard EA, Kucharik CJ, Monfreda C, Patz JA, Prentice IC, Ramankutty N, Snyder PK. 2005. Global consequences of land use. *Science* **309**: 570–574, doi: 10.1126/science.1111772.

Gao X, Zhang D, Chen Z, Pal JS, Giorgi F. 2007. Land use effects on climate in China as simulated by a regional climate model. *Sci. China D* **50**: 620–628, doi: 10.1007/s11430-007-2060-y.

Gent PR, Danabasoglu G, Donner LJ, Holland MM, Hunke EC, Jayne SR, Lawrence DM, Neale RB, Rasch PJ, Vertenstein M, Worley PH, Yang ZL, Zhang M. 2011. The Community Climate System Model Version 4. *J. Clim.* **24**: 4973–4991, doi: 10.1175/2011JCLI4083.1.

Goldewijk KK. 2001. Estimating global land use change over the past 300 years: The HYDE Database. *Global Biogeochem. Cycles* **15**: 417–433, doi: 10.1029/1999GB001232.

Goldewijk KK, Beusen A, Janssen P. 2010. Long-term dynamic modeling of global population and built-up area in a spatially explicit way: HYDE 3.1. *Holocene* **20**: 565–573, doi: 10.1177/0959683609356587.

Goldewijk KK, Beusen A, van Drecht G, de Vos M. 2011. The HYDE 3.1 spatially explicit database of human-induced global land-use change over the past 12,000 years. *Glob. Ecol. Biogeogr.* **20**: 73–86, doi: 10.1111/j.1466-8238.2010.00587.x.

Harrison R, Hester R. 2014. *Geoengineering of the Climate System*. Royal Society of Chemistry: Cambridge: UK.

He F, Vavrus SJ, Kutzbach JE, Ruddiman WF, Kaplan JO, Krumhardt KM. 2014. Simulating global and local surface temperature changes due to Holocene anthropogenic land cover change. *Geophys. Res. Lett.* **41**: 623–631, doi: 10.1002/2013GL058085.

Hegerl GC, Zwiers FW, Stott PA, Kharin VV. 2004. Detectability of anthropogenic changes in annual temperature and precipitation extremes. *J. Clim.* **17**: 3683–3700, doi: 10.1175/1520-0442(2004)017<3683:DOACIA>2.0.CO;2.

Hirsch AL, Pitman AJ, Kala J, Lorenz R, Donat MG. 2015. Modulation of land-use change impacts on temperature extremes via land–atmosphere coupling over Australia. *Earth Interact.* **19**: 1–24, doi: 10.1175/EI-D-15-0011.1.

Hu Y, Dong W, He Y. 2010. Impact of land surface forcings on mean and extreme temperature in eastern China. *J. Geophys. Res. Atmos.* **115**: D19117, doi: 10.1029/2009JD013368.

Hua W, Chen H. 2013a. Recognition of climatic effects of land use/land cover change under global warming. *Chin. Sci. Bull.* **58**: 3852–3858, doi: 10.1007/s11434-013-5902-3.

Hua W, Chen H. 2013b. Impacts of regional-scale land use/land cover change on diurnal temperature range. *Adv. Clim. Chan. Res.* **4**: 166–172, doi: 10.3724/SP.J.1248.2013.166.

Hua W, Chen H, Li X. 2015a. Effects of future land use change on the regional climate in China. *Sci. China Earth Sci.* **58**: 1840–1848, doi: 10.1007/s11430-015-5082-x.

Hua W, Chen H, Sun S, Zhou L. 2015b. Assessing climatic impacts of future land use and land cover change projected with the CanESM2 model. *Int. J. Climatol.* **35**: 3661–3675, doi: 10.1002/joc.4240.

Hurtt GC, Frolking S, Fearon MG, Moore B, Shevliakova E, Malyshev S, Pacala SW, Houghton RA. 2006. The underpinnings of land-use history: three centuries of global gridded land-use transitions, wood-harvest activity, and resulting secondary lands. *Glob. Change Biol.* **12**: 1208–1229, doi: 10.1111/j.1365-2486.2006.01150.x.

Hurtt GC, Chini LP, Frolking S, Betts R, Feedema J, Fischer G, Goldewijk KK, Hibbard K, Janetos A, Jones C. 2009. Harmonization of global land-use scenarios for the period 1500–2100 for IPCC-AR5. *iLEAPS Newsletter* **7**: 6–8.

Hurtt GC, Chini LP, Frolking S, Betts RA, Feddema J, Fischer G, Fisk JP, Hibbard K, Houghton RA, Janetos A, Jones CD, Kindermann G, Kinoshita T, Klein Goldewijk K, Riahi K, Shevliakova E, Smith S, Stehfest E, Thomson A, Thornton P, van Vuuren DP, Wang YP. 2011. Harmonization of land-use scenarios for the period 1500–2100: 600 years of global gridded annual land-use transitions, wood harvest, and resulting secondary lands. *Clim. Change* **109**: 117–161, doi: 10.1007/s10584-011-0153-2.

IPCC. 2012. *Managing the Risks of Extreme Events and Disasters to Advance Climate Change Adaptation. A Special Report of Working Groups I and II of the Intergovernmental Panel on Climate Change (IPCC*, Field CB, Barros V, Stocker TF, Qin D, Dokken DJ, Ebi KL, Mastrandrea MD, Mach KJ, PLattner GK, Allen SK, Tignor M, Midgley PM (eds). Cambridge University Press: Cambridge, UK and New York.

IPCC. 2013. *Climate Change 2013: The Physical Science Basis. Contribution of Working Group I to the Fifth Assessment Report of the Intergovernmental Panel on Climate Change*. Cambridge University Press: Cambridge, UK and New York.

Juang JY, Katul G, Siqueira M, Stoy P, Novick K. 2007. Separating the effects of albedo from eco-physiological changes on surface temperature along a successional chronosequence in the southeastern United States. *Geophys. Res. Lett.* **34**: L21408.

Kalnay E, Cai M. 2003. Impact of urbanization and land-use change on climate. *Nature* **423**: 528–531, doi: 10.1038/nature01675.

Lawrence PJ, Chase TN. 2010. Investigating the climate impacts of global land cover change in the community climate system model. *Int. J. Climatol.* **30**: 2066–2087, doi: 10.1002/joc.2061.

Lawrence D, Vandecar K. 2015. Effects of tropical deforestation on climate and agriculture. *Nat. Clim. Change* **5**: 27–36, doi: 10.1038/nclimate2430.

Lawrence DM, Oleson KW, Flanner MG, Fletcher CG, Lawrence PJ, Levis S, Swenson SC, Bonan GB. 2011. The CCSM4 land simulation, 1850–2005: assessment of surface climate and new capabilities. *J. Clim.* **25**: 2240–2260, doi: 10.1175/JCLI-D-11-00103.1.

Lawrence PJ, Feddema JJ, Bonan GB, Meehl GA, O'Neill BC, Oleson KW, Levis S, Lawrence DM, Kluzek E, Lindsay K, Thornton PE. 2012. Simulating the biogeochemical and biogeophysical impacts of transient land cover change and wood harvest in the Community Climate System Model (CCSM4) from 1850 to 2100. *J. Clim.* **25**: 3071–3095, doi: 10.1175/JCLI-D-11-00256.1.

Lee X, Goulden ML, Hollinger DY, Barr A, Black TA, Bohrer G, Bracho R, Drake B, Goldstein A, Gu L, Katul G, Kolb T, Law BE, Margolis H, Meyers T, Monson R, Munger W, Oren R, Paw UKT, Richardson AD, Schmid HP, Staebler R, Wofsy S, Zhao L. 2011. Observed increase in local cooling effect of deforestation at higher latitudes. *Nature* **479**: 384–387, doi: 10.1038/nature10588.

Luyssaert S, Jammet M, Stoy PC, Estel S, Pongratz J, Ceschia E, Churkina G, Don A, Erb K, Ferlicoq M, Gielen B, Grunwald T, Houghton RA, Klumpp K, Knohl A, Kolb T, Kuemmerle T, Laurila T, Lohila A, Loustau D, McGrath MJ, Meyfroidt P, Moors EJ, Naudts K, Novick K, Otto J, Pilegaard K, Pio CA, Rambal S, Rebmann C, Ryder J, Suyker AE, Varlagin A, Wattenbach M, Dolman AJ. 2014. Land management and land-cover change have impacts of similar magnitude on surface temperature. *Nat. Clim. Change* **4**: 389–393, doi: 10.1038/nclimate2196.

Ma D, Notaro M, Liu Z, Chen G, Liu Y. 2013. Simulated impacts of afforestation in East China monsoon region as modulated by ocean variability. *Clim. Dyn.* **41**: 2439–2450, doi: 10.1007/s00382-012-1592-9.

Mahmood R, Pielke RA, Hubbard KG, Niyogi D, Dirmeyer PA, McAlpine C, Carleton AM, Hale R, Gameda S, Beltrán-Przekurat A, Baker B, McNider R, Legates DR, Shepherd M, Du J, Blanken PD, Frauenfeld OW, Nair US, Fall S. 2014. Land cover changes and their biogeophysical effects on climate. *Int. J. Climatol.* **34**: 929–953, doi: 10.1002/joc.3736.

Myhre GD, Shindell FM, Bréon W, Collins J, Fuglestvedt J, Huang D, Koch JF, Lamarque D, Lee B, Mendoza T, Nakajima A, Robock G, Stephens T, Takemura , Zhang H. 2013. Anthropogenic and natural radiative forcing. In *Climate Change 2013: The Physical Science Basis. Contribution of Working Group I to the Fifth Assessment Report of the Intergovernmental Panel on Climate Change*, Stocker TF, Qin D, Plattner GK, Tignor M, Allen SK, Boschung J, Nauels A, Xia Y, Bex V, Midgley PM (eds). Cambridge University Press: Cambridge, UK and New York, 659–740.

Neale RB, Chen CC, Gettelman A, Lauritzen PH, Park S, Williamson DL, Conley AJ, Garcia R, Kinnison D, Lamarque JF. 2012. Description of the NCAR community atmosphere model (CAM 5.0). NCAR Tech. Note NCAR/TN-486+STR.

de Noblet-Ducoudré N, Boisier JP, Pitman A, Bonan GB, Brovkin V, Cruz F, Delire C, Gayler V, Hurk BJJM, Lawrence PJ, Molen MK, Müller C, Reick CH, Strengers BJ, Voldoire A. 2012. Determining robust impacts of land-use-induced land cover changes on surface climate over north America and Eurasia: results from the first set of LUCID experiments. *J. Clim.* **25**: 3261–3281, doi: 10.1175/JCLI-D-11-00338.1.

Oke TR. 1978. *Boundary Layer Climates*, 2nd edn. New York: Routledge.

Oleson KW, Lawrence DM, Gordon B, Flanner MG, Kluzek E, Peter J, Levis S, Swenson SC, Thornton E, Feddema J. 2010. Technical description of version 4.0 of the Community Land Model (CLM). NCAR Tech. Note NCAR/TN-478+STR.

Orlowsky B, Seneviratne S. 2012. Global changes in extreme events: regional and seasonal dimension. *Clim. Change* **110**: 669–696, doi: 10.1007/s10584-011-0122-9.

Pielke RA. 2005. Land Use and Climate Change. *Science* **310**: 1625–1626, doi: 10.1126/science.1120529.

Pielke RA, Pitman A, Niyogi D, Mahmood R, McAlpine C, Hossain F, Goldewijk KK, Nair U, Betts R, Fall S, Reichstein M, Kabat P, de Noblet N. 2011. Land use/land cover changes and climate: modeling analysis and observational evidence. *Clim. Change* **2**: 828–850, doi: 10.1002/wcc.144.

Pitman AJ, de Noblet-Ducoudré N, Cruz FT, Davin EL, Bonan GB, Brovkin V, Claussen M, Delire C, Ganzeveld L, Gayler V, van den Hurk BJJM, Lawrence PJ, van der Molen MK, Müller C, Reick CH, Seneviratne SI, Strengers BJ, Voldoire A. 2009. Uncertainties in climate responses to past land cover change: First results from the LUCID intercomparison study. *Geophys. Res. Lett.* **36**: L14814.

Pitman AJ, de Noblet-Ducoudré N, Avila FB, Alexander LV, Boisier JP, Brovkin V, Delire C, Cruz F, Donat MG, Gayler V, van den Hurk B, Reick C, Voldoire A. 2012. Effects of land cover change on temperature and rainfall extremes in multi-model ensemble simulations. *Earth Syst. Dynam.* **3**: 213–231, doi: 10.5194/esd-3-213-2012.

Pongratz J, Reick CH, Raddatz T, Claussen M. 2008. A reconstruction of global agricultural areas and land cover for the last millennium. *Global Biogeochem. Cycles* **22**: GB3018.

Pongratz J, Reick CH, Raddatz T, Claussen M. 2010. Biogeophysical versus biogeochemical climate response to historical anthropogenic land cover change. *Geophys. Res. Lett.* **37**: L08702.

Ramankutty N, Foley JA. 1999. Estimating historical changes in global land cover: croplands from 1700 to 1992. *Global Biogeochem. Cycles* **13**: 997–1027, doi: 10.1029/1999GB900046.

Rosenberg NJ, Blad BL, Verma SB. 1983. *Microclimate: The Biological Environment*. Wiley: New York.

Seneviratne SI, Nicholls N, Easterling D, Goodess CM, Kanae S, Kossin J, Luo Y, Marengo J, McInnes K, Rahimi M, Reichstein M, Sorteberg A, Vera C, Zhang X. 2012. Changes in Climate Extremes and their Impacts on the Natural Physical Environment. In *Managing the Risks of Extreme Events and Disasters to Advance Climate Change*

Adaptation. A Special Report of Working Groups I and II of the Intergovernmental Panel on Climate Change (IPCC), Field CB, Barros V, Stocker TF, Qin D, Dokken DJ, Ebi KL, Mastrandrea MD, Mach KJ, PLattner GK, Allen SK, Tignor M, Midgley PM (eds). Cambridge University Press: Cambridge, UK and New York, 109–230.

Seneviratne SI, Donat MG, Mueller B, Alexander LV. 2014. No pause in the increase of hot temperature extremes. *Nat. Clim. Change* **4**: 161–163, doi: 10.1038/nclimate2145.

Sillmann J, Kharin V, Zhang X, Zwiers F, Bronaugh D. 2013a. Climate extremes indices in the CMIP5 multimodel ensemble: Part 1. Model evaluation in the present climate. *J. Geophys. Res. Atmos.* **118**: 1716–1733, doi: 10.1002/jgrd.50203.

Sillmann J, Kharin VV, Zwiers FW, Zhang X, Bronaugh D. 2013b. Climate extremes indices in the CMIP5 multimodel ensemble: part 2. Future climate projections. *J. Geophys. Res. Atmos.* **118**: 2473–2493, doi: 10.1002/jgrd.50188.

Sun Y, Zhang X, Zwiers FW, Song L, Wan H, Hu T, Yin H, Ren G. 2014. Rapid increase in the risk of extreme summer heat in Eastern China. *Nat. Clim. Change* **4**: 1082–1085, doi: 10.1038/nclimate2410.

Tebaldi C, Hayhoe K, Arblaster J, Meehl G. 2006. Going to the extremes. *Clim. Change* **79**: 185–211, doi: 10.1007/s10584-006-9051-4.

Voldoire A, Royer JF. 2004. Tropical deforestation and climate variability. *Clim. Dyn.* **22**: 857–874, doi: 10.1007/s00382-004-0423-z.

Wilhelm M, Davin EL, Seneviratne SI. 2015. Climate engineering of vegetated land for hot extremes mitigation: an earth system model sensitivity study. *J. Geophys. Res. Atmos.* **120**: 2612–2623, doi: 10.1002/2014JD022293.

Xu Z, Mahmood R, Yang ZL, Fu C, Su H. 2015. Investigating diurnal and seasonal climatic response to land use and land cover change over monsoon Asia with the Community Earth System Model. *J. Geophys. Res. Atmos.* **120**: 1137–1152, doi: 10.1002/2014JD022479.

Zhang H, Gao X, Li Y. 2009. Climate impacts of land-use change in China and its uncertainty in a global model simulation. *Clim. Dyn.* **32**: 473–494, doi: 10.1007/s00382-008-0388-4.

Zhang X, Alexander L, Hegerl GC, Jones P, Tank AK, Peterson TC, Trewin B, Zwiers FW. 2011. Indices for monitoring changes in extremes based on daily temperature and precipitation data. *Clim. Change* **2**: 851–870, doi: 10.1002/wcc.147.

Zhang M, Lee X, Yu G, Han S, Wang H, Yan J, Zhang Y, Li Y, Ohta T, Hirano T, Kim J, Yoshifuji N, Wang W. 2014. Response of surface air temperature to small-scale land clearing across latitudes. *Environ. Res. Lett.* **9**: 1748–9326, doi: 10.1088/1748-9326/9/3/034002.

Zhang W, Xu Z, Guo W. 2016. The impacts of land-use and land-cover change on tropospheric temperatures at global and regional scales. *Earth Interact.* **20**: 1–23, doi: 10.1175/EI-D-15-0029.1.

Zhou L, Dickinson RE, Tian Y, Fang J, Li Q, Kaufmann RK, Tucker CJ, Myneni RB. 2004. Evidence for a significant urbanization effect on climate in China. *Proc. Natl. Acad. Sci. USA* **101**: 9540–9544, doi: 10.1073/pnas.0400357101.

